



ELSEVIER

Chemical Engineering Science ■■■ (■■■) ■■■-■■■

Chemical
Engineering Science

www.elsevier.com/locate/ces

Roll compaction of a pharmaceutical excipient: Experimental validation of rolling theory for granular solids

G. Bindhumadhavan^a, J.P.K. Seville^{a,*}, M.J. Adams^a, R.W. Greenwood^a, S. Fitzpatrick^b

^aCentre for Formulation Engineering, Department of Chemical Engineering, The University of Birmingham, Edgbaston, Birmingham B15 2TT, UK

^bMerck Sharp and Dohme Ltd., Hertford Road, Hoddesdon, Herts EN11 9BU, UK

Abstract

Roll compaction is widely used in industry to produce free flowing agglomerates from a fine particulate feed. Two of the main advantages of this process are that it is dry and continuous. Despite being superficially a simple process, a quantitative understanding has proved difficult to develop because of the complex behaviour of particulate materials. Sub-optimal design and operation of the equipment can lead to unsatisfactory products. Johanson (1965, ASME, Journal of Applied Mechanics Series E, 32(4), 842–848) developed a theoretical model that enables the surface pressure, torque and separating force of the rolls to be predicted from the physical characteristics of the powder and the dimensions of the rolls. However, a detailed experimental validation of the theory has yet to be accomplished. The current paper describes such a study using a gravity fed instrumented roll press and a microcrystalline cellulose powder. The measured pressure profiles in the nip region of the roll press were comparable to the calculated values. The theory was also found to predict the effect of material properties on the nip angle and the peak pressure but it was unable to account for the influence of roll speed.

© 2005 Published by Elsevier Ltd.

Keywords: Roll compactor; Dry granulation; Pharmaceutical excipient; Rolling theory

1. Introduction

Roll compaction is a continuous dry granulation process that is widely employed in the pharmaceutical, chemical and mineral industries in order to manufacture free flowing agglomerates. The feed powder is passed through two counter-rotating rolls with the flow being induced by the friction acting at the surfaces of the rolls. In the narrow region of the gap between the rolls, the powder is subjected to high pressure, leading to the formation of a compact or briquette (see Fig. 1 that is reduced in size by milling or screening to achieve the desired granule size.

Roll compaction is designed to increase the bulk density and uniformity of particulate formulations, for example, to prevent the segregation of pharmaceutical drugs. It offers unique advantages compared with wet granulation for processing physically or chemically moisture-sensitive

materials since the use of a liquid binder is not required. Another advantage is that it does not require a drying stage and therefore it is suitable for compounds that either have a low melting point or degrade rapidly upon heating (Pietsch, 1991; Miller, 1997; Seville et al., 2001). However, a roll compaction process can generate a temperature increase of 30 °C, limiting the advantage of this process.

It is usual to consider that there are three zones of material behaviour in roll compaction, which correspond to the *slip*, *nip* and *release* regions (Johanson, 1965). The boundaries between the regions are defined by their angular positions (see Fig. 1). The slip or entry region occurs before the nip region and is characterized by the feed particles slipping at the roll surface. Particle rearrangement and de-aeration can occur, but the pressures exerted on the powder are relatively small. The effectiveness of the slip region is related to the wall friction and inter-particle friction of the feed powder. The start of this region is defined by the entry angle, θ_h , which corresponds to the angular position at which there is a finite roll pressure. The nip region starts at a roll angle α ,

* Corresponding author. Tel.: +44 121 414 53 22; fax: +44 121 414 53 77.
E-mail address: j.p.k.seville@bham.ac.uk (J.P.K. Seville).



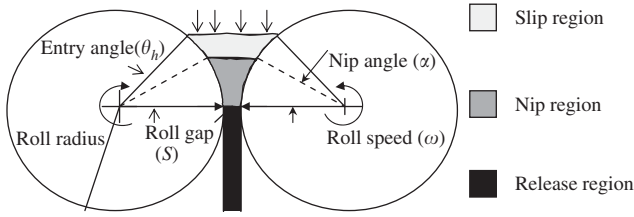


Fig. 1. Schematic diagram of the roll compaction process.

1 termed the *nip angle*, when the wall velocity of the powder
 2 becomes equal to that of the rolls. The powder is ‘nipped’
 3 and densification occurs due to the reduction in the gap as
 4 the powder is dragged to the point of closest approach. This
 5 results in a substantial increase in the roll pressure. The
 6 release region is initiated when the roll gap starts to increase
 7 again. The size of this region depends on the stored elastic
 8 strains in the compact, the rate at which it is released and
 9 the roll speed.

10 The process of powder deformation during roll compaction
 11 is not completely understood at a quantitative level. The
 12 friction between the rolls and the material, which largely
 13 controls the compaction, is difficult to measure directly
 14 and only with special instrumentation it is possible to
 15 measure the operating roll surface pressure. In the slip
 16 and nip regions, the powder becomes distorted in an almost
 17 unpredictable way while passing between the rolls. The
 18 powder spreads depending on the dimensions of the rollers,
 19 the nature of the powder and also on the surface conditions
 20 of the roll and roll speed.

21 A number of researchers have explored the roll compaction
 22 process by different approaches (Johanson, 1965;
 23 Katashinskii, 1986; Dec, 1991; Odagi et al., 2001; Dec et
 24 al., 2003). Katashinskii (1986) developed a slab analysis
 25 method to predict the pressure distribution and roll separation
 26 force in metal powder rolling processes. The method
 27 requires input data (namely the neutral angle at which the
 28 wall friction vector changes direction) from the experimen-
 29 tally measured pressure profile. Dec (1991) discussed the
 30 discrepancies and inconsistencies in the predicted data from
 31 this method. Odagi et al. (2001) described the application
 32 of a two-dimensional discrete element method (DEM) simu-
 33 lation that was based on the formulation developed by Tsuji
 34 et al. (1992). This involved the Hertz and Mindlin theories
 35 to compute the normal and tangential forces, respectively.
 36 Odagi et al. (2001) introduced an interaction law to allow
 37 for inter-particle adhesion and powder cohesiveness. How-
 38 ever, the model was found to under-predict the measured
 39 pressures in the nip region by many orders of magnitude.
 40 Dec et al. (2003) reviewed the various available models and
 41 argued that an improved predictive capability should be ob-
 42 tainable using finite element analysis. However, it was con-
 43 cluded that more accurate material models were required for
 the satisfactory implementation of this procedure.

Johanson (1965) developed an analytical model that en-
 45 ables the roll surface pressure, force and torque to be pre-
 46 dicted from the physical characteristics of the powder and
 47 the dimensions of the rolls. The main advantage of this
 48 model is that it requires only a limited number of experi-
 49 mental parameters for the powder: namely the angle of wall
 50 friction and the angle of internal friction (both measurable
 51 from shear testing experiments) and a compressibility fac-
 52 tor (determined from the uniaxial compression). However, a
 53 detailed experimental validation has yet to be accomplished
 54 and this was the aim of the current work by using an instru-
 55 mented roll press.

2. Theory

Johanson’s (1965) model was based on the Jenike yield
 57 criteria for steady-state particle flow in silos and hoppers.
 58 The material is assumed to be isotropic, frictional, cohesive
 59 and compressible and also to obey the effective yield func-
 60 tion proposed by Jenike and Shield (1959). For the plane
 61 strain condition between the rollers, the effective yield func-
 62 tion can be represented as in Fig. 2. The yield locus was
 63 combined with the equilibrium equations to give a system of
 64 partial hyperbolic differential equations, which can be solved
 65 using appropriate boundary conditions. Assuming slip oc-
 66 curs along the roll surfaces in the feed region, he showed
 67 that the pressure gradient ($d\sigma/dx$) in the slip region is given
 68 by the following relationship: :
 69

$$\left(\frac{d\sigma}{dx}\right)_{\text{Slip}} = \frac{4\sigma((\pi/2) - \theta - \nu) \tan \delta_E}{(D/2)[1 + (S/D) - \cos \theta][\cot(A - \mu) - \cot(A + \mu)]}, \quad (1)$$

70 where θ is the angular position at the surface of a roll, such
 71 that $\theta = 0$ corresponds to the minimum gap, and the param-
 72 eter A is given by

$$A = \frac{\theta + \nu + (\pi/2)}{2}. \quad (2)$$

73 The acute angle (ν) between the tangent to the roll surface
 74 and the direction of the major principal stress σ_1 is given by
 75 (see Fig. 2)

$$2\nu = \pi - \arcsin \frac{\sin \phi_w}{\sin \delta} - \phi_w. \quad (3)$$

76 In the nip region, a simplified material model was applied.
 77 It was assumed that no slip occurring along the roll surface
 78 and all material trapped between the two rollers at the nip
 79 angle must be compressed into a compact with a thickness
 80 equal to the roll gap. For smooth rollers, the pressure σ_θ
 81 at any $\theta < \alpha$ is related to the pressure at the nip angle σ_α
 82 by
 83
 84
 85

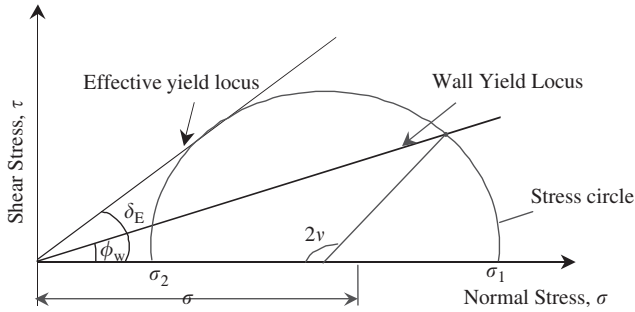


Fig. 2. Jenike–Shield yield criterion for the slip region.

1 the following pressure–density relationship:

$$\sigma_\theta = \sigma_\alpha \left[\frac{\rho_\theta}{\rho_\alpha} \right]^K = \sigma_\alpha \left[\frac{(1 + (S/D) - \cos \alpha) \cos \alpha}{(1 + (S/D) - \cos \theta) \cos \theta} \right]^K, \quad (3)$$

3 where K is the compressibility factor that is determined from
5 the slope of logarithmic plots of the density as a function of
7 pressure in uniaxial compaction.

7 The pressure gradient for the nip condition is given by

$$\left(\frac{d\sigma}{dx} \right)_{\text{Nip}} = \frac{K \sigma_\theta (2 \cos \theta - 1 - (S/D)) \tan \theta}{(D/2)[(1 + (S/D) - \cos \theta) \cos \theta]}. \quad (4)$$

9 Johanson (1965) proposed that the pressure gradients in the
11 slip and nip regions are equal at the nip angle, α , thus

$$\left(\frac{d\sigma}{dx} \right)_{\text{Slip}} = \left(\frac{d\sigma}{dx} \right)_{\text{Nip}}. \quad (5)$$

13 The point of intersection of the pressure gradient curves
15 (see Fig. 7) corresponds to the nip angle. Hence, α can be
17 deduced by solving Eqs. (1) and (4)

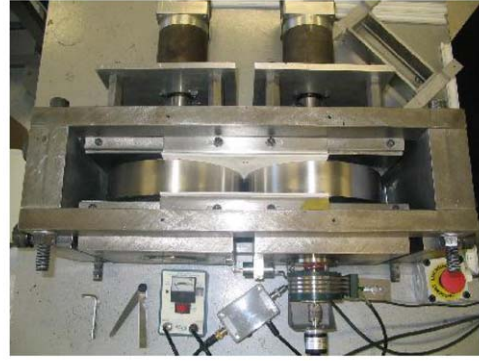
$$\frac{4((\pi/2) - \alpha - \nu) \tan \delta_E}{[\cot(A - \mu) - \cot(A + \mu)]} = \frac{K(2 \cos \alpha - 1 - (S/D)) \tan \alpha}{\cos \alpha}. \quad (6)$$

19 Thus the nip angle depends on the compressibility factor,
21 K , the material flow properties, δ_E , ϕ_w , the roll diameter D
23 and the roll gap S .

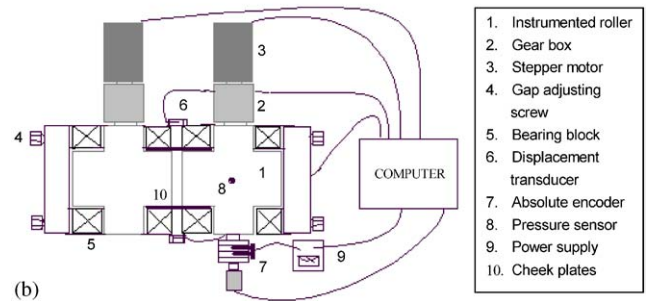
3. Experimental

3.1. Instrumented roll compactor

21 In the current work, a purpose built gravity fed roll compactor
23 (Fig. 3) was used. It consists of a fixed axis solid
25 roller and a movable instrumented roller, each machined
27 from stainless steel. The dimensions of the rollers are: di-
ameter 20 cm and face width 4.6 cm. They are driven by
stepper motors that are controlled using the LabVIEW pro-
gram (National Instruments, UK). The motors are driven by



(a)



(b)

Fig. 3. (a) Laboratory scale instrumented roll compactor. (b) Schematic layout of the instrumented roll compactor.

a single quartz oscillator unit (McLennan Servo Supplies Ltd, UK; model PM160), which ensures a precise setting of the roller speed. An external clock was used to transmit the same impulse frequency to both motors, ensuring simultaneous rotation. The roll speed can be varied from 0.5 to 20 rpm. In order to prevent leakage of the material, the sides of the rolls were sealed using cheek plates.

The instrumented roller is fitted with a miniature piezoelectric transducer (PCB Piezotronics Inc, USA; model 105C33) in order to measure the pressure profile normal to the roll surface; it was specified for a maximum pressure of 120 MPa. This involved the use of a specially segmented roller for accommodating the transducer. The signals from the transducer were transmitted by means of a slip ring assembly to a computer via an analog/digital converter card (National Instruments, UK; model SCB 68). The gap between the rolls can be varied from 0 to 5 mm, which was measured by using two LVDT displacement transducers (Solatron Metrology, UK; model Dfg5). An absolute encoder that was mechanically coupled to the instrumented roller shaft was employed to measure the angular position of the pressure transducer simultaneously with the pressure measurement. A rectangular hopper was used to feed the powder into the rollers. Experiments were carried out at ambient conditions. Although Avicel PH102 is sensitive to humidity and temperature, no significant systematic variations of the data were observed due to fluctuations in the ambient conditions.

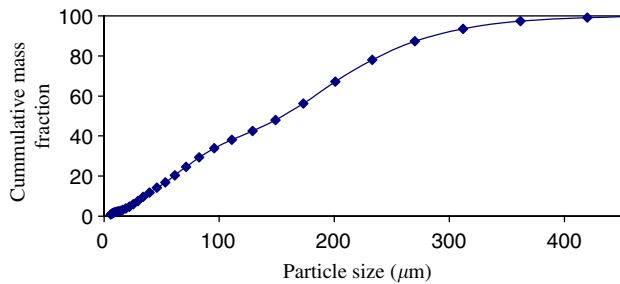
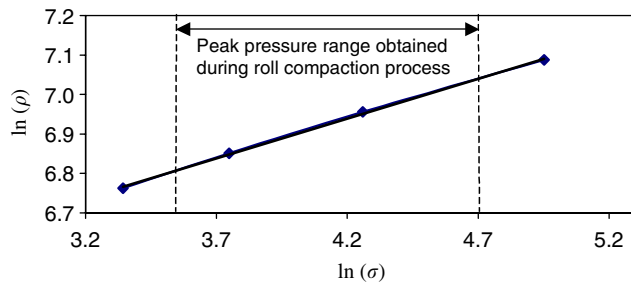


Fig. 4. Particle size distribution of Avicel PH102.

Fig. 5. Determination of compressibility factor (K).

3.2. Powder characterisation

Microcrystalline cellulose grade Avicel PH102 (FMC Biopolymer, USA), which is a commonly used excipient in tablet formulations, was used as a model material. The particle size distribution was measured using a particle size analyser (Sympatec, Helos model). The analyser is based on the laser diffraction principle and it is a dry measurement technique. The sample was fed into the measurement zone using an air injector set to a pressure of 2 bar. It was found that the particles had a wide size distribution with a mean value (d_{50}) of 105 μm as shown in Fig. 4.

A Peschl[®] rotational split level shear tester was used to measure the flow properties of the powder. The method of operation is based on the principle of rotational shearing. The standard shear testing procedure was used to measure the effective angle of internal friction and angle of wall friction (Peschl and Colijn, 1977). Measurements were made at three different consolidation loads. The effective angle of internal friction, δ_E , and the angle of wall friction (against stainless steel), ϕ_w , were found to be 40.5° and 18°, respectively.

The compressibility factor was measured by compacting samples of mass 2 g in a tableting cell with an internal diameter of 35 mm. This was carried out using an Instron testing machine (model 1195) with maximum pressures ranging from 10 to 100 MPa and a constant compaction rate of 20 mm/min. The bulk densities, ρ , of the compacts produced at different compaction pressures, σ , were measured. The compressibility factor was found to be 4.97 from a logarithmic plot of ρ as a function of σ (see Fig. 5).

4. Results and discussion

A typical pressure profile for a roll gap of 1.2 mm and a roll speed 2 rpm is shown in Fig. 6. The nip angle was obtained from such data as the intersection of two tangents drawn through the profile as shown in Fig. 6. The peak pressure was also taken directly from the measured profile. The predictions from Johanson's theory were compared with these experimental results. The nip angle determined from the experimental pressure profile was compared with the value predicted by the theory using Eq. (6) and also with the value obtained from the predicted pressure profile, which will be discussed later.

Eq. (6) was solved analytically using the laboratory test results, namely compressibility factor ($K=4.97$), inter-particle friction and wall friction ($\delta_E = 40.5^\circ$ and $\phi_w = 18^\circ$). The solution is represented graphically in Fig. 7 for a roll gap of 1.2 mm (corresponding to an S/D ratio of 0.006) and a roll speed of 2 rpm from which the nip angle was found to be 10°. The calculations were repeated for different roll gaps and for the same roll speed but the calculated nip angles were found to be almost independent of the gap because the effect of the ratio S/D in Eq. (6) is small. The nip angles were also measured experimentally for the same roll gaps and roll speed; the results are presented in Fig. 8. It may be seen that for small roll gaps, the nip angle increases with the gap and decreases at greater values of the gap. However, the maximum difference between the two sets of values is only about 1°. Moreover, it is important to note that the nip angle, as defined theoretically, may not be identical with

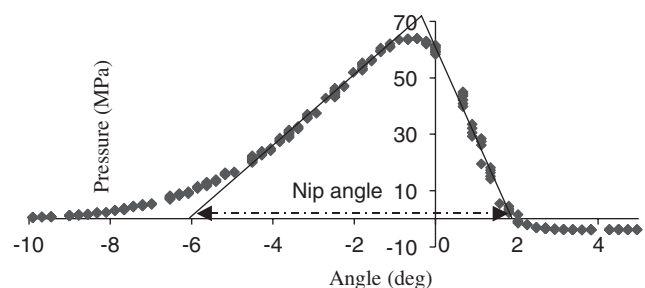


Fig. 6. Typical pressure profile (Avicel PH102, 1.2 mm gap, 2 rpm speed).

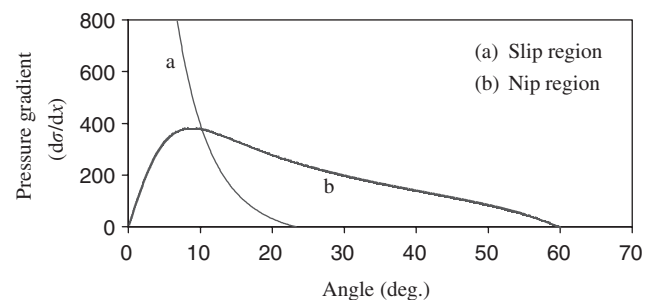


Fig. 7. Determination of nip angle (roll gap: 1.2 mm, roll speed: 2 rpm).

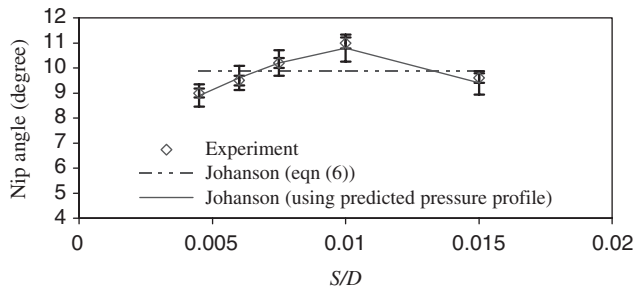


Fig. 8. Comparison of the predicted and experimental nip angles.

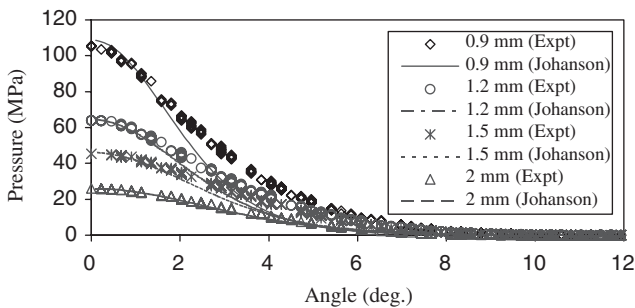


Fig. 9. Effect of the roll gap on the pressure profile: the curves were calculated from Johanson's theory.

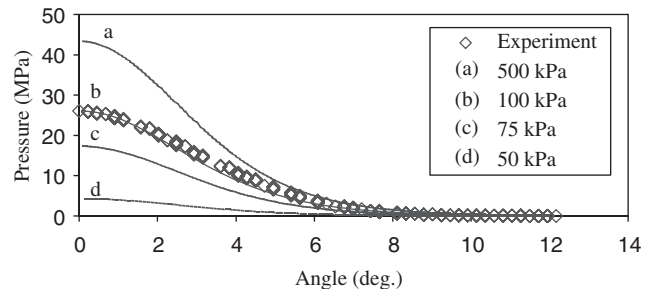


Fig. 10. The experimental pressure profile for a roll gap of 1.2 mm and a roll speed of 2 rpm: the curves show the influence of the nip pressure on the calculated pressure profile.

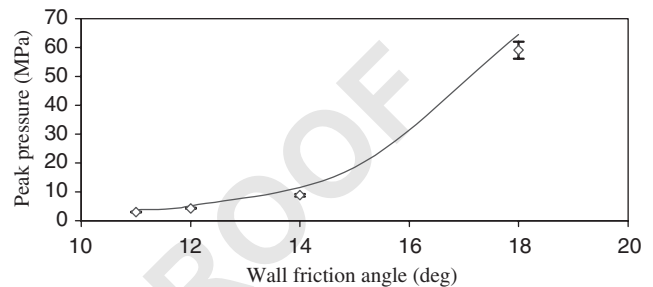


Fig. 11. The effect of wall friction on the peak pressure for a roll gap of 1.2 mm and a roll speed of 2 rpm: the curve was calculated from Johanson's theory.

that derived experimentally, which is taken as the angle of initiation of the pressure increase detected by the pressure sensor. To some extent, the accuracy of this result depends upon the sensitivity of the sensor.

The roll surface pressure profile in the nip region for the gap of 1.2 mm was calculated using Eq. (3). The pressure at the nip (σ_z) was taken to be 0.1 MPa, which corresponds to the minimum detectable voltage reading (~ 0.01 V) of the transducer system. This value cannot be predicted theoretically but is in a similar range to that used for previous calculations, Johanson (1977). Fig. 9 shows a comparison of the measured and calculated pressure profiles and it may be seen that there is reasonably close agreement. However, it should be emphasised that the nip pressure is essentially a fitting parameter because of the considerable sensitivity of the pressure profile to relatively small changes in the value, as shown in Fig. 10.

The nip angles were also obtained from the calculated pressure profiles using Eq. (3) and the results are given in Fig. 8. These data are in much closer agreement with the measured nip angles obtained from the experimental pressure profiles than those calculated using Eq. (6).

Experiments were carried out at different initial roll gaps and at a fixed roll speed of 2 rpm in order to understand the effect of the gap on the pressure profile. The measured and calculated profiles are shown in Fig. 9. There is excellent agreement for the peak pressures but the measured values increase more rapidly as the powder enters the nip region particularly as the minimum gap becomes smaller. It is pos-

sible that the deviations resulted from the roll gap approaching that of the particle size.

The inter-particle and wall frictions play significant roles in the performance of the roll compaction process. In particular, the size of the feed and compaction zones depend on the frictional behaviour of the material. To study the influence of roll surface friction, experiments were carried out using Avicel PH102 samples lubricated with different amounts of magnesium stearate (Mallinckrodt, USA), which was blended using a laboratory double cone mixer (Kemutec, UK) for 2 min at 50 rpm. The wall friction angles for the differently lubricated samples were measured using the Peschl shear tester. The effect of this angle on the peak pressure was calculated from Johanson's model and compared with the experimental results (see Fig. 11). The peak pressure increases substantially with increasing wall friction and there is close agreement between theory and experiment.

Johanson's model does not explicitly take account of the effect of roll speed. However, to understand the influence of this parameter, experiments were carried out at different roll speeds for three roll gaps and the peak pressures were measured. The results are plotted in Fig. 12 and show that the peak pressures are in excellent agreement with the theory at slow speeds. However, the nip pressure decreases with increasing roll speed. There was also a corresponding reduction in the strength of the compacts with increasing roll speeds, which is consistent with a greater entrainment of air.

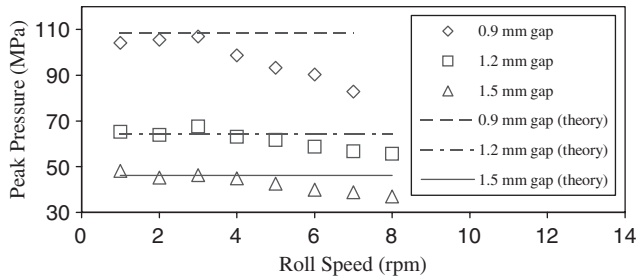


Fig. 12. The effect of roll speed on the peak pressure at different roll gaps: the lines were calculated from Johanson's theory.

In summary, the current work has shown that Johanson's model is able to provide a reasonable basis for calculating the nip angle and pressure profiles developed in a roll press for a gravity fed system. In principle, the current findings will apply to a screw fed system but the additional complexity of a fluctuating feed pressure (Guigon and Simon, 2003) needs to be considered. The major weakness of the model is the need to estimate the nip pressure since the complete pressure profile is very sensitive to this parameter. However, this boundary condition is likely to be a problem for any model unless a detailed analysis of the feed region is included. Such an extension might be able to account for the entrainment of air that results in a roll speed dependence of the roll pressure and which is ignored in Johanson's model. Further work is required to validate the predictions of roll separation force and roll torque with appropriate instrumentation.

It has been argued previously by Sommer and Hauser (2003) that such developments are required, including the use of a more complex material model. The disadvantage is that considerably more effort is required to measure the associated material parameters as is the case for the use of numerical solutions obtained using finite element analysis, for example.

5. Conclusions

An attempt was made to validate the model of Johanson for the roll compaction of powders by undertaking measurements with an instrumented device that incorporated a piezoelectric pressure transducer. The measured roll pressures increased somewhat more rapidly than the predicted values as the powder passes through the nip region, with the difference increasing with decreasing values of the minimum gap. However, the model quite accurately predicted the peak pressures obtained using a gravity fed roll compactor. The measured nip angles depended slightly on the roll gap but the calculated value, which is independent of the gap, is a reasonable estimate. The model quite accurately predicts the influence of roll speed on the peak pressures except that it does not account for the reduction in the pressure at increasing speed due to air entrainment.

Notation

D	roll diameter, m
K	compressibility constant for granular solid, dimensionless
S	roll gap, m

Greeks letters

α	nip angle, deg
δ	angle of internal friction, deg
δ_E	effective angle of internal friction, deg
θ	angular roll position, deg
θ_h	angular position at which feed pressure is applied, deg
μ	friction coefficient, dimensionless
ν	acute angle, deg
ρ_α	bulk density at position $\theta = \alpha$, kg/m ³
ρ_θ	bulk density at position θ , kg/m ³
σ	normal stress, Pa
σ_α	normal stress $\theta = \alpha$, Pa
σ_θ	normal stress at $\theta = \theta$, Pa
τ	shear stress, Pa
ϕ_w	angle of wall friction, deg

6. Uncited reference

Perera (2003).

Acknowledgements

The authors wish to acknowledge financial support from Merck Sharp and Dohme Ltd, Hertfordshire, UK. G. Bindhumadhavan wishes to express his sincere thanks to Mr. Bob Sharp and Mr. Derek Green for instrumentation of the roll compaction rig.

References

- Dec, R.T., 1991. Study of compaction process in roll press. Proceedings of the Institute for Briquetting and Agglomeration 22, 207–218. 47
- Dec, R.T., Zavaliangos, A., Cunningham, J.C., 2003. Comparison of various modeling methods for analysis of powder compaction in roller press. Powder Technology 130, 265–271. 49
- Guigon, P., Simon, O., 2003. Roll press design—influence of force feed systems on compaction. Powder Technology 130, 41–48. 51
- Jenike, A.W., Shield, R.T., 1959. On the plastic flow of Coulomb solids beyond original failure. Journal of Applied Mechanics, Transactions of the ASME 81, Series E 26, 599–602. 53
- Johanson, J.R., 1965. A rolling theory for granular solids. ASME, Journal of Applied Mechanics Series E 32 (4), 842–848. 55
- Johanson, J.R., 1977. Use of theory for design and selection of roll presses for agglomeration and compaction. In: Agglomeration 77, pp. 678–694, Chapter 36. 57
- Katashinskii, V.P., 1986. Analytical determination of specific pressure during the rolling of metal powders. Soviet Powder Metallurgy and Metal Ceramics 10, 765–772 (in Russian). 59

- 1 Miller, R., 1997. Roller compaction technology. In: Parikh, D.M. (Ed.),
3 Handbook of Pharmaceutical Granulation Technology. Marcel Dekker,
New York, pp. 99–150.
- 5 Odagi, K., Tanaka, T., Tsuji, Y., 2001. Compressive flow property of
7 powder in roll-type presses—Numerical simulation by discrete element
method. *Journal of the Society of Powder Technology* 38, 150–159
(in Japanese).
- 9 Perera, L.N., 2003. Roll compaction of pharmaceutical excipients. Ph.D
Thesis, The University of Birmingham.
- 11 Peschl, I.A.S.Z., Colijn, H., 1977. New rotational shear testing technique.
Journal of Powder & Bulk Solids Technology 1, 55–60.
- Pietsch, W., 1991. *Size Enlargement by Agglomeration*. Wiley, New York.
- 13 Seville, J.P.K., Perera, L.N., Greenwood, R.W., Bentham, C., 2001. Roll
granulation: principles and applications. In: Van der poel, A.F.B. et al.
15 (Eds.), *Advances in Nutritional Technology 2001*. Wageningen Press,
Netherlands, pp. 71–82.
- 17 Sommer, K., Hauser, G., 2003. Flow and compression properties of feed
solids for roll-type presses and extrusion presses. *Powder Technology*
130, 272–276.
- 19 Tsuji, Y., Tanaka, T., Ishida, T., 1992. Lagrangian numerical simulation
of plug flow of cohesionless particles in a horizontal pipe. *Powder*
21 *Technology* 71, 239–250.

UNCORRECTED PROOF